Brittle-Quasibrittle Transition in Dynamic Fracture: An Energetic Signature

J. Scheibert,[1,2,*] C. Guerra,[1,3] F. Célarié,[1,2,†] D. Dalmas,[2] and D. Bonamy[1]

[1]CEA, IRAMIS, SPCSI, Group Complex Systems and Fracture, F-91191 Gif-sur-Yvette, France
[2]Unité Mixte CNRS/Saint-Gobain, Surface du Verre et Interfaces, 39 Quai Lucien Lefranc, 93303 Aubervilliers cedex, France
[3]Facultad de Ingeniería Mecánica y Eléctrica, Universidad Autónoma de Nuevo León, Avenida Universidad, S/N, Ciudad Universitaria, C.P. 66450, San Nicolás de los Garza, NL, Mexico

(Received 10 June 2009; published 27 January 2010)

Dynamic fracture experiments were performed in polymethylmethacrylate over a wide range of velocities and reveal that the fracture energy exhibits an abrupt threefold increase from its value at crack initiation at a well-defined critical velocity, below the one associated with the onset of microbranching instability. This transition is associated with the appearance of conics patterns on fracture surfaces that, in many materials, are the signature of damage spreading through the nucleation and growth of microcracks. A simple model allows us to relate both the energetic and fractographic measurements. These results suggest that dynamic fracture at low velocities in amorphous materials is controlled by the brittle-quasibrittle transition studied here.

DOI: 10.1103/PhysRevLett.104.045501 PACS numbers: 62.20.M−, 46.50.+a, 61.43.−j

Dynamic fracture drives catastrophic material failures. Over the past century, a coherent theoretical framework, the so-called linear elastic fracture mechanics (LEFM) has developed and provided a quantitative description of the motion of a single smooth crack in a linear elastic material [1]. LEFM assumes that all the mechanical energy released during fracturing is dissipated at the crack tip. Defining the fracture energy Γ as the energy needed to create two crack surfaces of a unit area, the instantaneous crack growth velocity v is then selected by the balance between the energy flux and the dissipation rate Γv. This yields [1]

$$\Gamma \simeq (1 - v/c_R)K^2(c)/E, \tag{1}$$

where c_R and E are the Rayleigh wave speed and the Young modulus of the material, respectively, and $K(c)$ is the stress intensity factor (SIF) for a quasistatic crack of length c. K depends only on the applied loading and specimen geometry and characterizes entirely the stress field in the vicinity of the crack front.

Equation (1) describes quantitatively the experimental results for dynamic brittle fracture at slow crack velocities [2]. However, large discrepancies are observed in brittle amorphous materials at high velocities [3–6]. In particular, (i) the measured maximum crack speeds lie in the range $0.5–0.6c_R$, i.e., far smaller than the limiting speed c_R predicted by Eq. (1), and (ii) fracture surfaces become rough at high velocities (see [3,4] for reviews). It has been argued [7] that experiments start to depart from theory above a critical $v_b \simeq 0.4c_R$ associated to the onset of microbranching instabilities [8]: for $v > v_b$ the crack motion becomes a multicrack state. This translates into (i) a dramatic increase of the fracture energy Γ at v_b, due to the increasing number of microbranches propagating simultaneously, and (ii) a nonunivocal relation between Γ and v [7]. The microbranching instability hence yielded many recent theoretical efforts [9]. However, a number of puzzling observations remain at smaller velocities. In particular, even for velocities much lower than v_b, (i) the measured dynamic fracture energy is generally much higher than that at crack initiation [7,10–12] and (ii) fracture surfaces roughen over length scales much larger than the microstructure scale (''mist'' patterns) [13], the origin of which remains debated [14,15].

In this Letter, we report dynamic fracture experiments in polymethylmethacrylate (PMMA), the archetype of brittle amorphous materials, designed to unravel the primary cause of these last discrepancies. We show that the dynamic fracture energy exhibits an abrupt threefold increase from its value at crack initiation at a well-defined critical velocity v_a well below v_b. This increase coincides with the onset of damage spreading through the nucleation and growth of microcracks, the signature of which is the presence of conic patterns on the postmortem fracture surfaces. A simple model for this nominally brittle to quasibrittle transition is shown to reproduce both the energetic and fractographic measurements.

Dynamic cracks are driven in PMMA with measured Young modulus and Poisson ratio of $E = 2.8 \pm 0.2$ GPa and $\nu = 0.36$, which yields $c_R = 880 \pm 30\ \mathrm{m \cdot s^{-1}}$. Its fracture energy at the onset of crack propagation was determined to be $K_c^2/E = 0.42 \pm 0.07\ \mathrm{kJ \cdot m^{-2}}$, with K_c being the material toughness. Specimens are prepared from $140 \times 125 \times 15\ \mathrm{mm^3}$ parallelepipeds in the x (propagation), y (loading), and z (thickness) directions by cutting a $25 \times 25\ \mathrm{mm^2}$ rectangle from the middle of one of the $125 \times 15\ \mathrm{mm^2}$ edges and then cutting a 10 mm groove deeper into the specimen (Fig. 1, bottom inset). Two steel jaws equipped with rollers are placed on both sides of the cutout rectangle and a steel wedge (semiangle 15°) is pushed between them at constant velocity $38\ \mu\mathrm{m \cdot s^{-1}}$ up to crack initiation. In this so-called wedge-splitting geometry, the SIF K decreases with the crack length c.

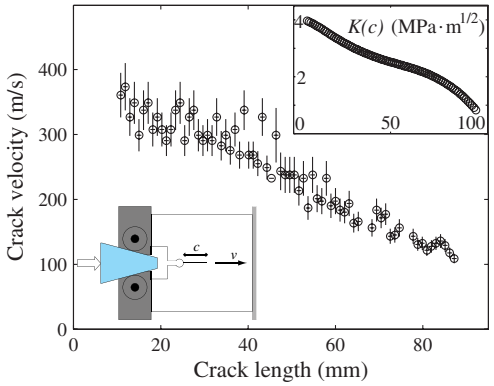

FIG. 1 (color online). Measured crack velocity v as a function of crack length c in a typical experiment ($U_0 = 2.6$ J). The vertical lines are error bars. Top inset: Calculated quasistatic SIF K as a function of c. Bottom inset: Schematics of the wedge-splitting test.

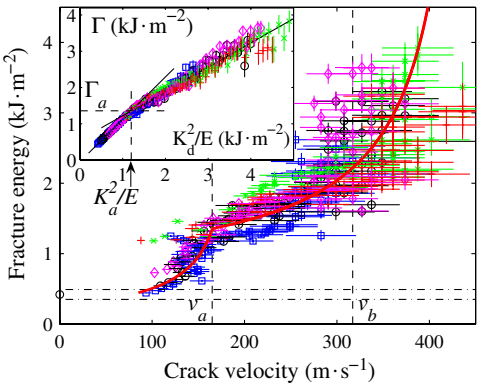

FIG. 2 (color online). Fracture energy Γ as a function of crack velocity v for five different experiments with different stored mechanical energies U_0 at crack initiation: 2.0 (□), 2.6 (○), 2.9 (◇), 3.8 (+), and 4.2 J (×). The two vertical dashed lines correspond to v_a and v_b. The two horizontal dashed lines indicate the confidence interval for the measured fracture energy K_c^2/E at crack initiation. The thick gray (red) line is the curve $\Gamma(v)$ obtained by combining Eqs. (1) and (2) for $v \leq v_a$ and Eqs. (1) and (4) for $v \geq v_a$. The correlation coefficient between this curve and the experimental points is $R = 0.83$. Inset: Γ as a function of K_d^2/E (see model) for the same experiments. A crossover between two linear regimes (linear fits in black lines) occurs at $K_d^2/E = K_a^2/E \simeq 1.2\,\mathrm{kJ\cdot m^{-2}}$, $\Gamma = \Gamma_a \simeq 1.34\,\mathrm{kJ\cdot m^{-2}}$.

To increase its value at crack initiation, and therefore the initial crack velocity, a circular hole with a radius ranging between 2 and 8 mm is drilled at the tip of the groove to tune the stored mechanical energy U_0. Dynamic crack growth with instantaneous velocities ranging from 75 to 500 $\mathrm{m\cdot s^{-1}}$ and stable trajectories are obtained. The location $c(t)$ of the crack front is measured during each experiment (40 μm and 0.1 μs resolutions) using a modified version of the potential drop technique: A series of 90 parallel conductive lines (2.4 nm-thick Cr layer covered with 23 nm-thick Au layer), 500 μm wide with an x period of 1 mm are deposited on one of the x-y surfaces of the specimen, connected in parallel and alimented with a voltage source. As the crack propagates, the conductive lines are cut at successive times, these events being detected with an oscilloscope. The instantaneous crack velocity $v(c)$ is computed from $c(t)$, and the instantaneous SIF $K(c)$ is calculated using 2D finite element calculations (software CASTEM 2007) on the exact experimental geometry, assuming plane stress conditions and a constant wedge position as boundary condition.

Values for the fracture energy Γ are obtained directly from Eq. (1) by combining the v measurements and the K calculations. Typical $v(c)$ and $K(c)$ curves are shown in Fig. 1. The variations of Γ with v (Fig. 2) are found to be the same in various experiments performed with various stored mechanical energy $U_0 > 2.0$ J at crack initiation. This curve provides evidence for three regimes, separated by two critical velocities. For slow crack velocities, Γ remains of the order of K_c^2/E as expected in LEFM. Then, as v reaches the first critical velocity $v_a \simeq 165\ \mathrm{m\cdot s^{-1}} = 0.19 c_R$, Γ increases abruptly to a value about 3 times larger than K_c^2/E. Beyond v_a, Γ increases slowly with v up to the second critical velocity, $v_b = 0.36 c_R \simeq 317\ \mathrm{m\cdot s^{-1}}$ [7], above which Γ diverges again with v. This second increase corresponds to the onset of the microbranching instability, widely discussed in the literature [7,8], whereas the first one, at v_a, is reported here for the first time. The high slope of $\Gamma(v)$ around v_a provides a direct interpretation for the repeated observation of cracks that span a large range of Γ but propagate at a nearly constant velocity of about $0.2 c_R$ (see, e.g., Refs. [16,17]).

The postmortem fracture surfaces shed light on the nature of the transition at $v = v_a$ on the curve $\Gamma(v)$. Figure 3 shows the surface morphology for increasing crack velocity. For $v < v_a$, the fracture surfaces remain smooth at the optical scale [Fig. 3(a), top]. Above v_a conic marks are observed [Figs. 3(b) and 3(c), top]. They do not leave any visible print on the sides of the specimens [Fig. 3(b), bottom], contrary to the microbranches that develop for $v \geq v_b$ [Fig. 3(c), bottom].

Similar conic marks were reported in the fracture of many other amorphous brittle materials (see [4,13] and references therein), including polymer glasses, silica glasses, and polycrystals. Their formation is thought to

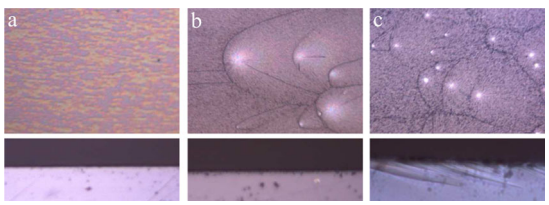

FIG. 3 (color online). Microscope images (×10) taken at (a) $v = 120 \pm 20\ \mathrm{m\cdot s^{-1}}$, $K^2/E = 1\ \mathrm{kJ\cdot m^{-2}}$, (b) $v = 260 \pm 30\ \mathrm{m\cdot s^{-1}}$, $K^2/E = 2\ \mathrm{kJ\cdot m^{-2}}$, (c) $v = 650 \pm 100\ \mathrm{m\cdot s^{-1}}$, $K^2/E = 7\ \mathrm{kJ\cdot m^{-2}}$. Top line: Fracture surfaces ($0.5 \times 0.7\ \mathrm{mm^2}$ field of view). Bottom line: Sample sides ($0.25 \times 0.7\ \mathrm{mm^2}$ field of view). Crack propagation is from left to right.

arise from inherent toughness fluctuations at the microstructure scale due to material heterogeneities randomly distributed in the material [17,18]. The enhanced stress field in the vicinity of the main crack front activates some of the low toughness zones and triggers the initiation of secondary penny-shaped microcracks ahead of the crack front. Each microcrack grows radially under the stress associated with the main crack along a plane different from it. When two cracks intersect in space and time, the ligament separating them breaks up, leaving a visible conic marking on the postmortem fracture surface.

Figure 4 shows the surface density of conic marks ρ as a function of crack velocity v. Below v_a, no conic mark is observed up to $\times 50$ magnification, consistent with [19]. Above v_a, ρ increases almost linearly with $v - v_a$. The exact correspondence between the critical velocity v_a at which Γ exhibits an abrupt increase and the velocity at which the first conic marks appear on the fracture surfaces strongly suggests that both phenomena arc associated with the same transition. The nucleation and growth of microcracks can therefore be identified as the new fracture mechanism that starts at v_a. This damage process is generic in brittle materials and is relevant for an even wider range of materials than those that exhibit conic marks, e.g., granite [20].

We now present a simple model reproducing the $\Gamma(v)$ curve between 0 and v_b. We assume that linear elasticity fails in the material when the local stress reaches a yield stress σ_Y. It defines a fracture process zone (FPZ) around the crack tip, the size of which is given by $R_c(v) = K_d^2(c, v)/a\sigma_Y^2$, where a is a dimensionless constant [15] and K_d is the dynamic SIF. We consider that all the dissipative phenomena (plastic deformations, crazing or cavitation for instance) occur in the FPZ, with a volume dissipated energy ϵ. The material is then assumed to contain a volume density ρ_s of discrete "source sinks" (SS, see e.g., [15] for previous uses of this concept). Each SS is assumed to activate into a microcrack if two conditions are met: (i) the local stress reaches σ_Y and (ii) the SS is located at a distance from the crack tip larger than d_a [21]. The nucleation of a microcrack is assumed to be accompanied by an excluded volume V where stress is screened, i.e., no SS can activate anymore. In the following, ρ_s, σ_Y, ϵ, d_a, and V are taken as constants throughout the material. Three cases should be considered.

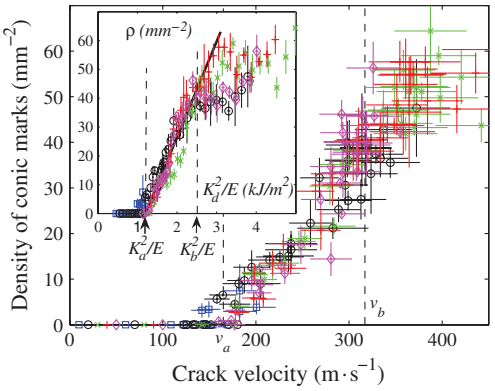

FIG. 4 (color online). Surface density ρ of conic marks as a function of crack velocity for all experiments shown in Fig. 2. Inset: ρ as a function of K_d^2/E (linear fit in black line).

(I) At the onset of crack propagation, all the volume within $R_c(v = 0) = K_c^2/a\sigma_Y^2$ contributes to the fracture energy $\Gamma(v = 0) = K_c^2/E$.

(II) For $v \leq v_a$, no microcrack nucleates and $R_c(v) = K_d(c, v)^2/a\sigma_Y^2 < d_a$. The dynamic SIF is then $K_d(c, v) = k(v)K(c)$ [1], where $k(v) \simeq (1 - v/c_R)/\sqrt{1 - v/c_D}$ is universal and c_D is the dilatational wave speed (here $c_D = 2010 \pm 60$ m · s^{-1}). The volume scanned by the FPZ when the crack surface increases by S is $2R_c(v)S$. The dissipated energy $\Gamma(v)S$ is given by $\gamma S + 2\epsilon R_c(v)S$, where γ is the Griffith surface energy. Since $\Gamma(v = 0) = K_c^2/E$, one finally gets for $v \leq v_a$:

$$\Gamma(v) = \alpha \frac{K_d(v)^2}{E} + (1 - \alpha)\frac{K_c^2}{E} \quad \text{with} \quad \alpha = \frac{2\epsilon E}{a\sigma_Y^2}. \quad (2)$$

This predicted linear dependence of Γ with K_d^2/E for $v \leq v_a$ is in agreement with measurements (Fig. 2, inset). A linear fit to the data (correlation coefficient $R = 0.985$) gives $\alpha = 1.17 \pm 0.05$ and $K_c^2/E = 0.3 \pm 0.2$ kJ/m^2, where $\pm$ stands for 95% confidence interval. The latter value is compatible with the measurements of the fracture energy at crack initiation. By combining Eqs. (1) and (2), one gets a prediction for the $\Gamma(v)$ curve [22] that reproduces very well the low velocity regime in Fig. 2. Extrapolation of this regime [22] exhibits a divergence of the dissipated energy for a finite velocity $v_a' = (\alpha - 1)c_R c_D/(\alpha c_D - c_R) \simeq 200$ m · s^{-1} $\simeq 0.23 c_R$, slightly larger than v_a. In the absence of microcracks, this velocity v_a' would have therefore set the limiting macroscopic crack velocity.

(III) For $v \geq v_a$, $R_c(v) \geq d_a$, i.e., microcracks start to nucleate. The surface density of microcracks $\rho(v)$ is then equal to the number of activated SS beyond d_a per unit of fracture area, i.e., $\rho_s\{2[R_c(v) - R_c(v_a)] - \rho V\}$, where the last term stands for the excluded sites around microcracks. This yields

$$\rho(v) = \beta \frac{K_d(v)^2 - K_a^2}{E} \quad \text{with} \quad \beta = \frac{2E}{a\sigma_Y^2} \frac{\rho_s}{1 + \rho_s V}, \quad (3)$$

where $K_a = K_d(v_a)$. This linear relationship is in good agreement with the measurements for $\rho(K_d^2/E)$ before the microbranching onset, beyond which ρ saturates (Fig. 4, inset). A fit to the data ($R = 0.877$) between K_a and $K_b = K_d(v_b)$ gives $\beta = 33 \pm 3$ J^{-1}. In the microcracking regime, the local dynamic SIF K_d is not equal to the macroscopic one anymore, but corresponds to that at the individual microcrack tips, at which the limiting velocity is expected to be $v_a' \gtrsim v_a$. It is then natural to assume that all microcracks propagate at the same velocity v_a, which yields $K_d(v) = k(v_a)K$ [23]. The energy $\Gamma(v)S$ dissipated when the crack surface increases by S is $\gamma S + \epsilon[2R_c(v)S - \rho(v)SV]$, yielding

$$\Gamma(v) = \Gamma_a + \chi \frac{K_d(v)^2 - K_a^2}{E} \quad \text{with} \quad \chi = \frac{2\epsilon E/a\sigma_Y^2}{1 + \rho_s V}, \tag{4}$$

where $\Gamma_a = \Gamma(v_a)$. Equation (4) predicts a linear dependence of Γ with K_d^2/E, in agreement with the measurements for $K_d^2/E > K_a^2/E$ (Fig. 2, inset). A linear fit ($R = 0.948$) to the data between K_a and $K_b = K_d(v_b)$ gives $\chi = 0.67 \pm 0.01$. The corresponding predicted $\Gamma(v)$ curve [22] reproduces very well the intermediate velocity regime $v_a < v < v_b$ (Fig. 2) and exhibits a divergence of the dissipated energy for $v_\infty = c_R[1 - \chi k(v_a)^2] \simeq 450\ \mathrm{m \cdot s^{-1}} \simeq 0.52 c_R$. This limiting velocity is very close to the observed maximum crack speed in brittle amorphous materials.

This simple scenario allows us to illustrate how material defects control the dynamic fracture of amorphous solids before the onset of microbranching. For $v < v_a$, the mechanical energy released at the crack tip is dissipated into both a constant surface energy and a volume energy within the FPZ, the size of which increases with crack speed. With this mechanism alone, the crack speed would be limited to a value slightly larger than v_a. But damage spreading through microcracking makes it possible to observe much larger velocities: The crack propagates through the nucleation, growth, and coalescence of microcracks, with a macroscopic effective velocity that can be much larger than the local velocity of each microcrack tip [17,24]. We suggest that microcracks in themselves do not increase dissipation, but rather decrease it by locally screening the stress. At velocities larger than v_b, microbranches contribute to the dissipated energy proportionally to their surface [25]. We emphasize that the nominally brittle to quasibrittle transition occurring at v_a is very likely to be generic for amorphous solids and should therefore be taken into account in future conceptual and mathematical descriptions of dynamic fracture. In this respect, continuum damage mechanics [26] initially derived for "real" quasibrittle materials like ceramics or concrete may be relevant to describe fast crack growth in nominally brittle materials. In particular, a better understanding of the relationship between the dynamics of propagation of both the individual microcracks and the macroscopic crack is still needed.

We thank P. Viel and M. Laurent (SPCSI) for gold deposits, T. Bernard (SPCSI) for technical support, K. Ravi-Chandar (University of Texas, Austin) and J. Fineberg (The Hebrew University of Jerusalem) for fruitful discussions, and P. Meakin (INL/PGP) for a careful reading of the manuscript. We acknowledge funding from French ANR through Grant No. ANR-05-JCJC-0088 and from Mexican CONACYT through Grant No. 190091.

*Present address: PGP, University of Oslo, Oslo, Norway. julien.scheibert@fys.uio.no

†Present address: LARMAUR, Université de Rennes 1, Rennes, France.

[1] L. Freund, *Dynamic Fracture Mechanics* (Cambridge University Press, Cambridge, England, 1990).
[2] H. Bergkvist, Eng. Fract. Mech. **6**, 621 (1974).
[3] J. Fineberg and M. Marder, Phys. Rep. **313**, 1 (1999).
[4] K. Ravi-Chandar, *Dynamic Fracture* (Elsevier, Amsterdam, 2004).
[5] A. Livne, O. Ben-David, and J. Fineberg, Phys. Rev. Lett. **98**, 124301 (2007).
[6] A. Livne, E. Bouchbinder, and J. Fineberg, Phys. Rev. Lett. **101**, 264301 (2008).
[7] E. Sharon and J. Fineberg, Nature (London) **397**, 333 (1999).
[8] J. Fineberg *et al.*, Phys. Rev. Lett. **67**, 457 (1991).
[9] M. Adda-Bedia, Phys. Rev. Lett. **93**, 185502 (2004); H. Henry and H. Levine, Phys. Rev. Lett. **93**, 105504 (2004); E. Bouchbinder, J. Mathiesen, and I. Procaccia, Phys. Rev. E **71**, 056118 (2005); H. Henry, Europhys. Lett. **83**, 16 004 (2008).
[10] J. F. Kalthoff, S. Winkler, and J. Beinert, Int. J. Fract. **12**, 317 (1976).
[11] A. J. Rosakis, J. Duffy, and L. B. Freund, J. Mech. Phys. Solids **32**, 443 (1984).
[12] A. Bertram and J. F. Kalthoff, Materialprufung **45**, 100 (2003).
[13] D. Hull, *Fractography* (Cambridge University Press, Cambridge, England, 1999).
[14] J. W. Johnson and D. G. Holloway, Philos. Mag. **14**, 731 (1966); T. Cramer, A. Wanner, and P. Gumbsch, Phys. Rev. Lett. **85**, 788 (2000); D. Bonamy and K. Ravi-Chandar, Phys. Rev. Lett. **91**, 235502 (2003); M. J. Buehler and H. Gao, Nature (London) **439**, 307 (2006); G. Wang *et al.*, Phys. Rev. Lett. **98**, 235501 (2007); A. Rabinovitch and D. Bahat, Phys. Rev. E **78**, 067102 (2008).
[15] B. Lawn, *Fracture of Brittle Solids* (Cambridge University Press, Cambridge, England, 1993).
[16] K. Ravi-Chandar and W. G. Knauss, Int. J. Fract. **26**, 141 (1984).
[17] K. Ravi-Chandar and B. Yang, J. Mech. Phys. Solids **45**, 535 (1997).
[18] A. Smekal, Oesterr. Ing. Arch. **7**, 49 (1953).
[19] J. S. Sheng and Y. P. Zhao, Int. J. Fract. **98**, L9 (1999).
[20] D. K. Moore and D. A. Lockner, J. Struct. Geol. **17**, 95 (1995).
[21] We believe that conic marks correspond to the fraction of microcracks having sufficient time to develop up to optical scale. For too small FPZ (for $v \leq v_a$), nucleated microcracks are rapidly caught up by the main crack, only leaving undetectable submicrometric elliptic marks.
[22] C. Guerra *et al.* (to be published).
[23] This assumption was previously made ([17] and references therein) and is fully consistent with the observed shape of conic marks in our experiments [22].
[24] S. Prades *et al.*, Int. J. Solids Struct. **42**, 637 (2005).
[25] E. Sharon, S. P. Gross, and J. Fineberg, Phys. Rev. Lett. **76**, 2117 (1996).
[26] L. M. Kachanov, *Introduction to Continuum Damage Mechanics* (Martinus Nijhoff Publishers, Dordrecht, 1986).